ELSEVIER

Int. J. Radiation Oncology Biol. Phys., Vol. 41, No. 4, pp. 959–970, 1998
Copyright © 1998 Elsevier Science Inc.
Printed in the USA. All rights reserved
0360-3016/98 $19.00 + .00

PII S0360-3016(98)00150-3

● *Physics Contribution*

MONTE CARLO-BASED DOSE-RATE TABLES FOR THE AMERSHAM CDCS.J AND 3M MODEL 6500 ^{137}CS TUBES

JEFFREY F. WILLIAMSON, PH.D.*

*Radiation Oncology Center, Mallinckrodt Institute of Radiology, Washington University School of Medicine, St. Louis, MO 63110

Purpose: (1) To present reference-quality dose-rate distributions for the Amersham CDCS.J-type ^{137}Cs intracavitary source (hitherto unavailable in the literature) and updated tables for the 3M model 6500/6D6C source. (2) To assess the accuracy of the widely used 1D pathlength (Sievert integral) algorithm for lightly filtered ^{137}Cs tube sources.

Methods and Materials: A Monte Carlo photon-transport code is used to calculate the dose-rate distributions about the 3M source and the CDCS.J source based on radiographic examination of the sources and the vendors' specifications. Dose-rate distributions are provided in the form of Cartesian "away-and-along" lookup tables. Using a general form of the Sievert integral, calculated dose-rate distributions were compared to the Monte Carlo benchmark calculations treating the filtration coefficients as best-fit parameters as well as approximating them by linear energy absorption coefficients. In addition, the errors introduced by approximating the active source core by uniform cylinders or line sources was evaluated.

Results: The Model CDCS.J dose distribution differs from that of the 3M model 6500 source by −5.9% to +14.4% (root-mean-square [RMS] average: 2.6%). The RMS accuracy of the Sievert algorithm is 2.4% to 2.8% (error range of −1.4% to 7.6%) when filtration coefficients for steel and ceramic media are approximated by linear energy absorption coefficients. If the filtration coefficients are treated as parameters of best fit, selected to minimize the discrepancies between 1D pathlength and Monte Carlo calculations, the RMS error is reduced to 0.8% (error range of −1.8% to 4.1%). The optimal values of stainless steel and low-density ceramic or glass filtration coefficients are approximately independent of the source geometry.

Conclusions: The widely used Sievert integral algorithm accurately characterizes the dose distribution around stainless-steel clad low-density matrix ^{137}Cs sources, particularly if design-independent best-fit values of the filtration coefficients are used. Although both families of source designs studied produce similar dose distributions, source-design specific dose distributions should be used for clinical treatment planning and dose-algorithm validation. © 1998 Elsevier Science Inc.

^{137}Cs, Intracavitary sources, Dosimetry, Monte Carlo simulation.

INTRODUCTION

^{137}Cs, encapsulated in stainless steel tubes, is widely used for manual afterloading intracavitary brachytherapy. Accurate dose-rate tables, based on the geometric and mechanical specifications of each source type, are essential quality assurance tools. Such tables are needed to verify (1, 2) Sievert integral (1D pathlength) calculations (3, 4) used by most treatment planning systems for generating dose distributions. These tables are needed for those treatment planning systems which calculate dose by table lookup based upon user-supplied dose-rate distributions. Finally, such tabulated dose-rate distributions are useful for performing manual treatment-time calculations and for verifying graphical treatment plans.

The main purpose of this communication is to present detailed 2D dose-rate distributions for two widely used Amersham model CDCS.J and 3M model 6500 ^{137}Cs intracavitary sources, derived from an experimentally benchmarked Monte Carlo photon-transport (MCPT) code. Most manual-afterloading intracavitary treatments in the U.S. are carried out using one of these two source types. The 3M model 6500 source was introduced in 1967 (5) and was widely distributed until 1992, when its manufacture was discontinued. The most widely cited dose-rate tables for this source (6, 7) are over 20 years old. Although more recent 3M source tables, e.g. (8), are available, all are based upon the Sievert integral model. As of this writing, the Amersham CDCS.J source is the only commercially available intracavitary tube. Compared to the 3M source, the CDCS.J tube has a smaller external diameter, is encapsulated in 0.5 mm- rather than 1-mm-thick stainless steel, and has a slightly

Reprint requests to: Jeffrey F. Williamson, Ph.D., Radiation Oncology Center, Mallinckrodt Institute of Radiology, Washington University School of Medicine, St. Louis, MO 63110.

Acknowledgments—This work was supported by a research contract from NicoMed/Amersham and by a research grant (R01 CA46640) awarded by the National Institutes of Health. The author thanks Michael Langton, Ph.D. (Amersham Healthcare) and David Kubiatowicz (3M Co.) for providing information on the design of sources marketed by their respective companies.

Accepted for publication 27 March 1998.

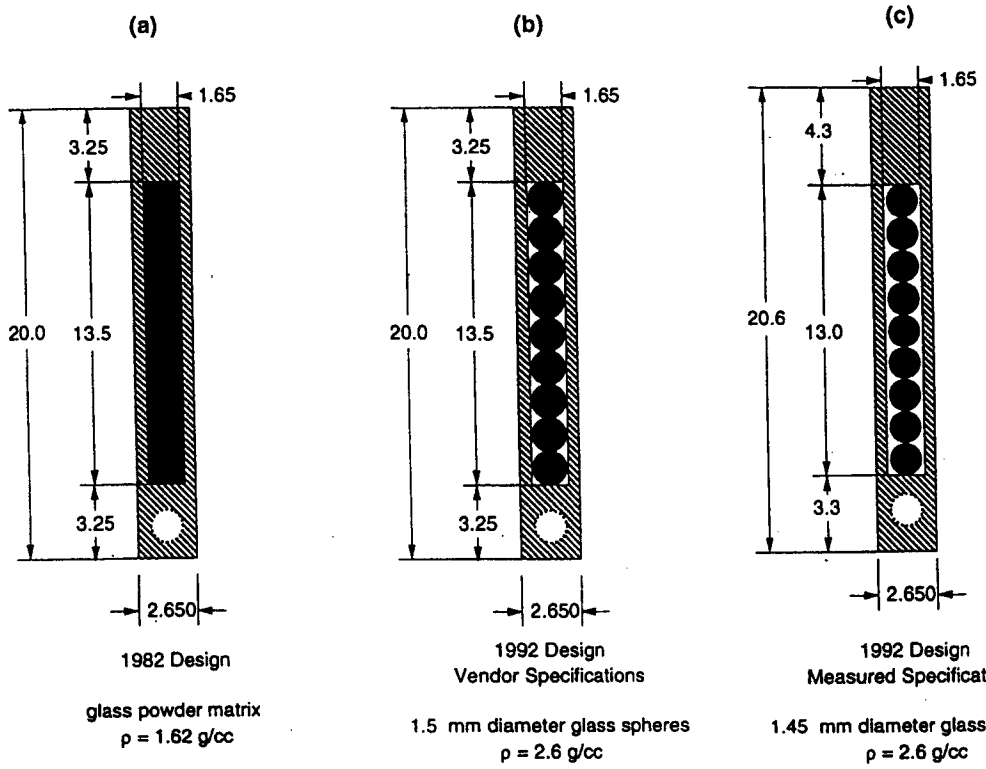

Fig. 1. (a) The CDCS.J source 1982 design geometry, consisting of a uniform glass cylinder placed symmetrically between source tips, as described in the vendor's literature. (b) Geometry of the CDCS.J 1992 design cesium-137 intracavitary tube, consisting of an array of nine ceramic beads placed symmetrically in the source capsule as described by the vendor's mechanical drawings. (c) The CDCS.J 1992 design intracavitary tube geometry based on average dimensions derived from transmission radiographs of 25 different sources. Compared to the vendor's specifications, the ceramic bead array is slightly shorter and is placed asymmetrically in the source capsule.

shorter active length. No complete dose–rate tables are available for the CDCS.J design, although Metcalfe (9) has published a partial table.

The second goal of this communication is to assess the 1D pathlength model accuracy relative to the Monte Carlo–based away-and-along dose-rate tables. Previous studies comparing the Sievert integral algorithm against dose measurements (9, 10) around ^{137}Cs sources suggest that 1D pathlength dose calculations are accurate within 10%, with discrepancies exceeding 5% occurring only near the long axis of the source. The one available Monte Carlo–Sievert integral comparison (4) is limited to a single polar profile at a fixed distance of 2 cm from the source center. In contrast, the current study employs a fine 2D calculation grid ranging from 0.25 cm to 7 cm from the source center. MCPT calculations can easily achieve statistical precisions of less than 1%, which is far superior than the ±5% uncertainty achievable by experimental dose-rate measurements (11). MCPT benchmarking can detect even small systematic errors in 1D pathlength model calculations, especially if they both use the same cross-section data and geometric models. Finally, optimal filtration coefficient values are identified which reduce the mean error of the pathlength model below the 1% level.

METHODS AND MATERIALS

Source characteristics

The CDCS.J source design has evolved significantly over the years. Initially, the J-tube was encapsulated in 0.5-mm-thick platinum–iridium alloy (12). In 1982, stainless-steel encapsulation was introduced (13). The modified radioactive matrix (Fig. 1a, Table 1) consisted of ^{137}Cs chloride mixed with zirconium phosphate powder which is sintered at high temperature. The resultant insoluble powder is loaded into a 13.5-mm-long by 1.65-mm-diameter cylindrical cavity encapsulated symmetrically in stainless steel (AISI 316L) with a wall thickness of 0.5 mm and a physical length of 20 mm. In 1992, a modified design (Fig. 1b, Table 1) was introduced, in which the cylindrical glass core was replaced by a linear array of 1.5-mm-diameter borosilicate glass beads with a density of 2.6 g · cm^{-3} in a stainless-steel capsule of identical dimensions.

Transmission radiographs of 25 different 1992 CDCS.J sources received in three shipments were obtained to validate vendor's design specifications. The total length, active length, bead diameter, and thicknesses of inactive material on the eyelet and noneyelet ends of the source were measured and averaged. Several measured dimensions (Table 1) deviated significantly from the vendor's specifications

Table 1. Measured and specified intracavitary tube dimensions

Parameter	Amersham CDCS.J 1982 model vendor's specification	Amersham CDCS.J 1992 model			3M 6500 vendor's specification
		Measured range	Measured mean†	Vendor's specification	
Physical length	20.0 mm	20.3–20.9 mm	20.6 ± 0.6 mm	20.0 mm	20.0 mm
Physical diameter	2.65	—	—	2.65 mm	3.05 mm
Active length	13.5	11.8–13.5 mm	13.0 ± 0.5 mm	13.5 mm	13.8 mm
Active diameter	1.65	1.4–1.5 mm	1.45 mm	1.50 mm	1.19 mm
Wall thickness	0.5	—	—	0.5 mm	0.93 mm
Eyelet end: physical to active tip	3.25	2.8–5.0 mm	3.3 ± 0.4 mm	3.25 mm	3.9 mm
Noneyelet end: physical to active tip	3.25	3.3–5.2 mm	4.3 ± 0.8 mm	3.35 mm	2.3 mm
No. of ceramic spheres in active core	—	9	9 ± 0	7	—

† Excluding three outlying sources (see text).

Three of the sources had significantly shorter (11.8–12.2 mm) active lengths compared to the vendor's specifications, with the remaining sources having active lengths varying from 12.5 to 13.5 mm. In addition, all 25 sources were found to contain 9 rather than 7 glass spheres as specified by the vendor's product literature. All sources exhibited some asymmetric positioning of the active source in the capsule. Figure 1c summarizes the average geometric model extracted from our radiographic measurements. Figure 1b illustrates the vendor-specified dimensions, corrected only for the number of glass spheres. Table 2 summarizes the composition and physical properties of the source materials.

Despite significant differences between the vendor's design specifications and our measurements, the vendor remains committed to manufacturing sources that accurately reflect their specifications (personal communication: Michael A. Langton, Amersham-Mediphysics, Dec. 1997). On the other hand, it is likely that sources manufactured in the early 1990s are more accurately described by our measured source dimensions. Thus, dose-rate tables based upon both our measurements and the vendor's geometric specifications are presented.

The active core of the 3M model 6500 source (Fig. 2) is a cavity packed with 50–100 μm diameter zirconium phosphate glass microspheres (14) within which radioactive cesium chloride is distributed. This glass (Table 2) has a density of 3.00 g · cm^{-3} (15) yielding an effective cylindrical core density of 2.22 g · cm^{-3} based upon a tetrahedral packing arrangement. Radiographic examination of three 3M 6500 tubes revealed no detectable deviation from the vendor's specifications.

Monte Carlo calculations

An MCPT code was used to calculate the dose-rate distribution in water about the brachytherapy sources illustrated by Figs. 1 and 2. Our Monte Carlo code (11, 16, 17) simulates photoelectric absorption (followed by characteristic X-ray emission) and pair production as well as coherent and incoherent scattering. The photon cross-section library, DLC-99, distributed by the Radiation Shielding Information Center (18) was used along with the mass energy absorption coefficients tabulated by Hubbell (19). The ^{137}Cs primary photon spectra from NCRP Report 58 (20) was used. Unlike the semiempirical Sievert model, MCPT models all photon collision dynamics giving rise to the scattering and diffusion of ionizing radiation, taking into

Table 2. Source encapsulation and core media

Component	Material	% Atomic composition	Bulk density	Packed density: cylindrical core approximation
Source capsule	AISI 316L stainless steel	Si (2%), Cr (20%), Mn (2%), Fe (67%), Ni (9%)	8.02 g · cm^{-3}	—
CDCS.J source core 1982 model	Packed zirconium phosphate powder	O (70%), P (20%), Zr (10%)	—	1.62 g · cm^{-3}
CDCS.J source core 1992 model	1.45-mm-diameter borosilicate glass beads	B (7%), O (64%), Na (1%), Al (1%), Si (26%)	2.60	1.73
3M 6500 source core	50–100 μm diameter zirconium phosphate glass microspheres	O (70%), P (20%), Zr (10%)	3.00	2.22

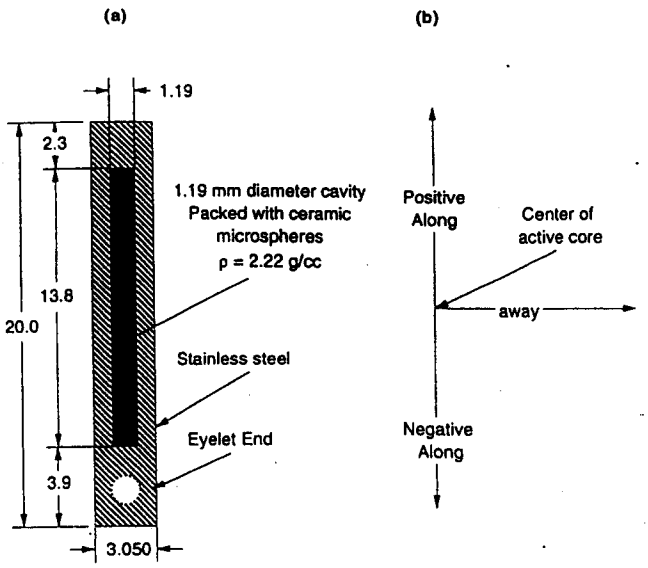

Fig. 2. (a) Geometry of the 3M Model 6500/6D6C cesium-137 intracavitary tube. The radioactive core consists of small ceramic microspheres which were simulated by a uniform ceramic cylinder with a packing density of 0.74. The wall thickness is 0.93 mm of stainless steel. (b) Illustration of the coordinate system used for Monte Carlo and Sievert calculations which is centered in the active core cavity rather than within the boundaries of the source capsule.

count the internal structure of the sources. This MCPT ode has been extensively tested against careful experimental measurements using thermoluminescent and diode detectors across the brachytherapy photon spectra ranging from ^{125}I to ^{137}Cs: agreement between MCPT simulation and the benchmark measurements ranges from 1–5% (21–24) in both homogeneous and heterogeneous measurement geometries.

For the CDCS.J 1992 measured and vendor-specified geometries, Monte Carlo simulations modeled their cores as 13.0- and 13.5-mm-long linear array of ceramic spheres (ρ = 2.60 g · cm^{-3}) placed end-to-end. The vendor-geometry simulation assumed symmetric positioning of the active length in the source capsule (3.25 mm from physical to active tip on each end) while the measured-geometry simulation assumed the asymmetric positioning illustrated in Fig. 1c. For the 1982 CDCS.J design, a symmetrically positioned, homogeneous cylindrical core with a density of 1.62 g · cm^{-3} and the dimensions shown in Fig. 1a were assumed. For the 3M 6500 source, a homogeneous cylindrical glass core with asymmetric positioning as illustrated by Fig. 2a was assumed. In all cases, the eyelet cavity was ignored.

For each source type, MCPT dose rates were obtained at approximately 317 points with the source positioned in the enter of a 30-cm-diameter liquid–water sphere. Calculation oints were arranged in a half plane, allowing for asymmetric positioning of active core between the physical tips of the capsule. The calculation plane extended 7 cm from the active core center in both the longitudinal (along) and transverse (away) directions with a 0.25-cm grid spacing near the source and 0.5 cm to 1 cm spacing further away. Simulation of 4,000,000 photon histories yielded total dose standard errors of the mean (68% confidence intervals) of less than 0.5%. The primary dose contribution (approximated by water kerma) was calculated by numerical integration of the isotropic point-source kernal (including inverse-square law, primary photon attenuation, and energy-fluence to kerma conversion summed over the photon spectrum) over the source volume, while the scattered-photon dose contribution was evaluated stochastically. The exponential track-length estimator (17) was used to score photon histories. The MCPT code neglected transport of secondary electrons, effectively approximating absorbed dose by collision kerma. Both analytical calculations (23) and coupled photon-electron Monte Carlo calculations (25) demonstrate that the errors introduced by this approximation are less than 1% at distances of 1 mm or more from the source capsule. As described elsewhere (11), the output of the code was normalized to unit air-kerma strength and represented by $[\dot{D}_{wat}(x,y)/S_K]_{MCPT}$ with units of cGy · h^{-1} per μGy · m^2 · h^{-1}.

1-D pathlength model (Sievert integral) calculations

Doses predicted by a Sievert integral model (generalized to accomodate 3D radioactivity distributions) were compared, point-by-point, to the MCPT-generated 2D dose-rate distribution. Because the Sievert algorithm and MCPT cal-

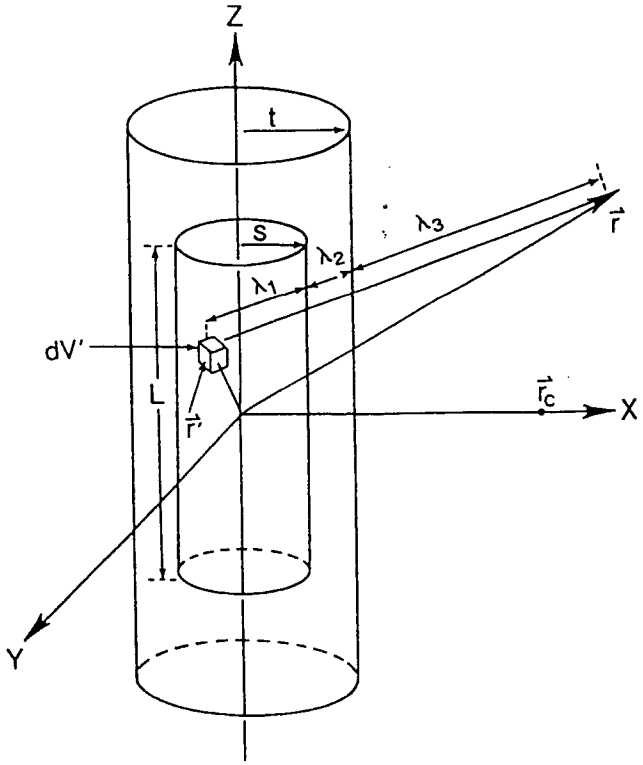

Fig. 3. Simplified geometry of a cylindrically symmetric encapsulated source, illustrating the 3D integration elements and ray tracing used to implement the 1D pathlength algorithm. (Reproduced from Ref. 26 with permission).

Table 3. Sievert integral filtration coefficients: ^{137}Cs tubes

Source material	Linear energy absorption coefficient	Best fit filtration coefficient
Stainless steel		
3M6500	0.0226 mm^{-1}	0.036 mm^{-1}
CDCS.J	0.0226 mm^{-1}	0.037 mm^{-1}
Source Core		
3M6500 (cylinder: 2.22 g/cc)	0.0065 mm^{-1}	0.0070 mm^{-1} (0.032 $cm^2\ g^{-1}$)
CDCS.J (spherical: 2.60 g/cc)	0.0076 mm^{-1}	—
CDCS.J (cylindrical: 1.73 g/cc)	0.0051 mm^{-1}	0.0046 mm^{-1} (0.027 $cm^2 \cdot g^{-1}$)

culations are based on the same 3D geometric model, all discrepancies can be unambiguously attributed to failure of the approximations underlying the 1D pathlength model. The 3D Sievert model, described in more detail elsewhere (4, 26), is only briefly described here. To illustrate the basic features of the model, assume that the radionuclide is uniformly distributed within an inner cylinder (active source) of active length, L, and radius, s, as shown in Fig. 3. The dose rate, $\dot{D}(\vec{r})$, in cGy/h at location $\vec{r}$ near the filtered source is given by:

$$\dot{D}(\vec{r}) = \frac{S_K \cdot (\overline{\mu_{en}/\rho})^{wat}_{air}}{F(\vec{r}_c)} \cdot \frac{1}{V} \int_V |\vec{r} - \vec{r}'|^{-2} \times \exp\left[-\sum_{j=1}^{3} \mu_j \cdot \lambda'_j\right] \cdot [1 + \mathrm{SPR}(\lambda'_3)] \cdot dV' \quad (1)$$

where V denotes space enclosed by the active source core. The indices $j = 1, \ldots, 3$ denote the media composing the active source core, the source encapsulation, and surrounding medium while λ'_1, λ'_2, and λ'_3 denote the corresponding distances traversed by primary photons passing from dV' to $\vec{r}$. The other symbols are defined as follows:

S_K = the air-kerma strength of the source in units of $\mu Gy \cdot m^2 \cdot h^{-1}$. It is the product of the air-kerma rate in free space, $\dot{K}_{air}(\vec{r}_c)$, at the reference point $\vec{r}_c$ in Fig. 3 and the square of the distance: $S_K = \dot{K}_{air}(\vec{r}_c) \cdot |\vec{r}_c|^2$.

$F(\vec{r}_c) = |\vec{r}_c|^2 \cdot 1/V \int_V |\vec{r}_c - \vec{r}'|^{-2} \cdot \exp(-\mu_1 \cdot \lambda'_1 - \mu_2 \cdot \lambda'_2) \cdot dV'$ corrects for self-absorption and filtration at the point assuming that the source is immersed in vacuum.

$(\overline{\mu_{en}/\rho})^{wat}_{air}$ = the ratio of mass–energy absorption coefficients, averaged over the photon spectrum in free space for water to that of air.

$\mathrm{SPR}(d) = \frac{\textit{scatter dose in water}}{\textit{primary dose in water}}$ at distance d from an isotropic point source having the same free-space spectrum as the actual encapsulated source.

μ_j = filtration coefficients of the active source and filter media for $j = 1$ and 2. In all of the calculations described in this report, μ_j is treated as a thickness-independent parameter. For the case of the surrounding liquid–water medium, $j = 3$, μ_3 is the linear attenuation coefficient of water, averaged over the primary photon spectrum.

Table 4. Amersham J-type intracavitary tube: dose rate per unit air-kerma strength [$cGy \cdot h^{-1}/(\mu Gy \cdot m^2 \cdot h^{-1})$] (1982 design: vendor-supplied specifications)

Distance along (cm)	Distance away (cm)													
	0.00	0.25	0.50	0.75	1.00	1.5	2.00	2.5	3.00	3.50	4.00	5.00	6.00	7.00
7.00	0.0187	0.0185	0.0182	0.0181	0.0182	0.0182	0.0179	0.0174	0.0167	0.0158	0.0149	0.0130	0.0112	0.00950
6.00	0.0260	0.0256	0.0252	0.0252	0.0254	0.0253	0.0246	0.0235	0.0221	0.0206	0.0191	0.0162	0.0135	0.0112
5.00	0.0383	0.0376	0.0369	0.0372	0.0374	0.0368	0.0351	0.0327	0.0301	0.0274	0.0248	0.0201	0.0162	0.0131
4.00	0.0614	0.0599	0.0591	0.0598	0.0597	0.0570	0.0525	0.0472	0.0419	0.0369	0.0324	0.0249	0.0193	0.0151
3.50	0.0814	0.0790	0.0786	0.0793	0.0785	0.0732	0.0656	0.0575	0.0498	0.0429	0.0369	0.0276	0.0209	0.0162
3.00	0.113	0.109	0.110	0.110	0.107	0.0962	0.0831	0.0705	0.0593	0.0498	0.0420	0.0304	0.0226	0.0172
2.50	0.167	0.160	0.162	0.160	0.152	0.130	0.107	0.0866	0.0704	0.0575	0.0474	0.0332	0.0241	0.0181
2.00	0.275	0.262	0.265	0.251	0.228	0.179	0.138	0.106	0.0828	0.0657	0.0529	0.0359	0.0256	0.0189
1.50	0.546	0.520	0.497	0.431	0.361	0.250	0.176	0.128	0.0957	0.0737	0.0581	0.0383	0.0268	0.0196
1.00	—	1.587	1.133	0.801	0.584	0.340	0.217	0.149	0.107	0.0806	0.0624	0.0402	0.0278	0.0201
0.50	—	6.690	2.484	1.351	0.854	0.426	0.252	0.165	0.116	0.0854	0.0653	0.0415	0.0284	0.0205
0.00	—	8.025	3.087	1.609	0.978	0.462	0.265	0.171	0.119	0.0870	0.0663	0.0419	0.0286	0.0206

To obtain cGy/mgRaEq-h, multiply table entries by 7.227.

Table 5. Amersham J-type intracavitary tube: dose rate per unit air-kerma strength [cGy · h^{-1}/(μGy · m^2 · h^{-1})]
(1992 design: symmetrically positioned active core approximation; vendor-supplied specifications)

Distance along (cm)	Distance away (cm)													
	0.00	0.25	0.50	0.75	1.00	1.5	2.00	2.5	3.00	3.50	4.00	5.00	6.00	7.00
7.00	0.0186	0.0186	0.0183	0.0182	0.0183	0.0183	0.0180	0.0175	0.0167	0.0159	0.0149	0.0130	0.0111	0.00945
6.00	0.0259	0.0258	0.0254	0.0254	0.0255	0.0254	0.0247	0.0236	0.0222	0.0207	0.0192	0.0161	0.0134	0.0111
5.00	0.0380	0.0379	0.0372	0.0374	0.0376	0.0370	0.0352	0.0329	0.0302	0.0275	0.0249	0.0201	0.0162	0.0130
4.00	0.0608	0.0604	0.0595	0.0602	0.0600	0.0573	0.0527	0.0474	0.0420	0.0370	0.0325	0.0249	0.0193	0.0151
3.50	0.0806	0.0798	0.0791	0.0798	0.0789	0.0735	0.0658	0.0577	0.0499	0.0430	0.0370	0.0276	0.0209	0.0161
3.00	0.112	0.110	0.110	0.110	0.107	0.0966	0.0834	0.0707	0.0594	0.0499	0.0421	0.0304	0.0225	0.0171
2.50	0.165	0.162	0.163	0.161	0.153	0.130	0.107	0.0868	0.0705	0.0576	0.0475	0.0332	0.0241	0.0181
2.00	0.271	0.264	0.266	0.252	0.229	0.180	0.138	0.106	0.0829	0.0657	0.0530	0.0359	0.0256	0.0189
1.50	0.539	0.522	0.500	0.434	0.363	0.250	0.176	0.128	0.0958	0.0737	0.0581	0.0383	0.0268	0.0196
1.00	—	1.589	1.141	0.805	0.585	0.341	0.218	0.149	0.108	0.0807	0.0625	0.0403	0.0278	0.0201
0.50	—	6.577	2.484	1.350	0.854	0.426	0.252	0.165	0.116	0.0854	0.0654	0.0415	0.0284	0.0205
0.00	—	8.084	3.087	1.612	0.979	0.463	0.266	0.171	0.119	0.0872	0.0664	0.0419	0.0286	0.0206

To obtain cGy/mgRaEq-h, multiply table entries by 7.227.

As explained in more detail elsewhere (26), eq. 1 was implemented by 3D numerical integration over the nine discrete glass spheres of Amersham source (1992 model), and, for the other sources, over the right cylindrical volume describing the ceramic or glass core.

Two methods of evaluating the filtration coefficients were considered. First, filtration coefficient were approximated (6, 10, 27) by the corresponding linear energy absorption coefficients: $\mu_j = \mu_{en,j}$. Their values (19) are listed in Table 3. Secondly, the μ_j were treated as parameters of best fit, and varied so as to find the pair of values $(\hat{\mu}_1, \hat{\mu}_2)$ that maximized the agreement between the 1D pathlength model and Monte Carlo calculations at the 317 simulated point detectors. To this end, a fine 2D filtration coefficient grid, (μ_1, μ_2), was defined (0.00 to 0.02 mm^{-1} for glass and 0.000 to 0.050 mm^{-1} for stainless steel) and the discrepancy between the Monte Carlo and 1D pathlength calculations at each pair of values quantified in terms of the relative root-mean square (RMS) standard deviation, $\%\sigma_{RMS}(\mu_1, \mu_2)$:

Table 6. Amersham J-type intracavitary tube: dose rate per unit air-kerma strength [cGy · h^{-1}/(μGy · m^2 · h^{-1})]
(1992 design: radiographically measured source geometry; asymmetrically placed active core)

Distance along (cm)	Distance away (cm)													
	0.00	0.25	0.50	0.75	1.00	1.5	2.00	2.5	3.00	3.50	4.00	5.00	6.00	7.00
7.00	0.0180	0.0181	0.0179	0.0179	0.0181	0.0182	0.0180	0.0175	0.0167	0.0159	0.0149	0.0130	0.0111	0.00942
6.00	0.0250	0.0250	0.0247	0.0249	0.0252	0.0253	0.0247	0.0236	0.0222	0.0207	0.0191	0.0161	0.0134	0.0111
5.00	0.0367	0.0367	0.0363	0.0369	0.0373	0.0368	0.0351	0.0328	0.0302	0.0275	0.0248	0.0201	0.0161	0.0130
4.00	0.0585	0.0584	0.0582	0.0595	0.0597	0.0571	0.0526	0.0473	0.0420	0.0370	0.0324	0.0249	0.0193	0.0151
3.50	0.0769	0.0767	0.0776	0.0791	0.0785	0.0733	0.0657	0.0576	0.0499	0.0430	0.0370	0.0276	0.0209	0.0161
3.00	0.107	0.106	0.108	0.110	0.107	0.0963	0.0832	0.0705	0.0593	0.0499	0.0420	0.0304	0.0225	0.0171
2.50	0.157	0.154	0.161	0.160	0.152	0.130	0.107	0.0866	0.0704	0.0575	0.0474	0.0332	0.0241	0.0180
2.00	0.258	0.255	0.264	0.251	0.228	0.179	0.138	0.106	0.0828	0.0657	0.0529	0.0359	0.0255	0.0189
1.50	0.507	0.509	0.494	0.429	0.360	0.250	0.176	0.128	0.0957	0.0737	0.0581	0.0383	0.0268	0.0196
1.00	—	1.525	1.118	0.796	0.584	0.340	0.218	0.149	0.107	0.0806	0.0624	0.0402	0.0278	0.0201
0.50	—	6.555	2.483	1.353	0.856	0.427	0.252	0.165	0.116	0.0854	0.0653	0.0415	0.0284	0.0205
0.00	—	8.290	3.138	1.629	0.985	0.464	0.266	0.171	0.119	0.0871	0.0663	0.0419	0.0286	0.0206
−0.50	—	6.547	2.481	1.353	0.856	0.427	0.252	0.165	0.116	0.0855	0.0654	0.0415	0.0284	0.0205
−1.00	—	1.524	1.117	0.797	0.584	0.341	0.218	0.149	0.108	0.0807	0.0625	0.0402	0.0278	0.0201
−1.50	0.528	0.513	0.493	0.428	0.361	0.250	0.176	0.128	0.0958	0.0738	0.0582	0.0384	0.0268	0.0196
−2.00	0.268	0.262	0.264	0.250	0.228	0.179	0.138	0.106	0.0829	0.0658	0.0530	0.0359	0.0256	0.0189
−2.50	0.163	0.161	0.162	0.160	0.152	0.130	0.107	0.0867	0.0705	0.0576	0.0475	0.0333	0.0241	0.0180
−3.00	0.111	0.110	0.110	0.110	0.107	0.0963	0.0833	0.0705	0.0594	0.0499	0.0421	0.0305	0.0226	0.0171
−3.50	0.0800	0.0797	0.0790	0.0796	0.0787	0.0733	0.0657	0.0576	0.0499	0.0430	0.0371	0.0277	0.0209	0.0161
.00	0.0607	0.0605	0.0595	0.0601	0.0599	0.0572	0.0526	0.0473	0.0420	0.0370	0.0324	0.0250	0.0193	0.0151
−5.00	0.0380	0.0380	0.0373	0.0374	0.0376	0.0369	0.0351	0.0328	0.0302	0.0275	0.0249	0.0201	0.0162	0.0131
−6.00	0.0258	0.0258	0.0254	0.0254	0.0255	0.0254	0.0247	0.0236	0.0222	0.0207	0.0191	0.0162	0.0135	0.0112
−7.00	0.0185	0.0186	0.0184	0.0182	0.0182	0.0183	0.0180	0.0175	0.0167	0.0159	0.0149	0.0130	0.0111	0.00947

To obtain cGy/mgRaEq-h, multiply table entries by 7.227.

Table 7. 3M Model 6500 intracavitary tube: dose rate per unit air-kerma strength [cGy · h^{-1}/(μGy · m^2 · h^{-1})]

Distance along (cm)	Distance away (cm)													
	0.00	0.25	0.50	0.75	1.00	1.5	2.00	2.5	3.00	3.50	4.00	5.00	6.00	7.00
7.00	0.0193	0.0189	0.0184	0.0180	0.0179	0.0178	0.0176	0.0170	0.0164	0.0156	0.0147	0.0129	0.0111	0.0094
6.00	0.0269	0.0263	0.0254	0.0249	0.0248	0.0247	0.0241	0.0231	0.0218	0.0204	0.0189	0.0160	0.0134	0.0112
5.00	0.0397	0.0386	0.0370	0.0365	0.0365	0.0359	0.0344	0.0322	0.0297	0.0272	0.0247	0.0201	0.0162	0.0131
4.00	0.0638	0.0614	0.0586	0.0584	0.0582	0.0559	0.0517	0.0468	0.0416	0.0367	0.0323	0.0249	0.0193	0.0151
3.50	0.0848	0.0811	0.0774	0.0773	0.0766	0.0719	0.0648	0.0570	0.0495	0.0428	0.0369	0.0276	0.0209	0.0162
3.00	0.118	0.112	0.107	0.107	0.105	0.0949	0.0824	0.0700	0.0591	0.0497	0.0420	0.0304	0.0226	0.0172
2.50	0.176	0.164	0.159	0.156	0.149	0.128	0.106	0.0863	0.0702	0.0575	0.0475	0.0332	0.0241	0.0181
2.00	0.290	0.265	0.257	0.246	0.225	0.178	0.137	0.106	0.0827	0.0657	0.0530	0.0359	0.0257	0.0189
1.50	0.580	0.516	0.489	0.427	0.360	0.249	0.176	0.128	0.0957	0.0737	0.0581	0.0383	0.0268	0.0196
1.00	—	1.580	1.135	0.799	0.582	0.340	0.217	0.149	0.107	0.0807	0.0625	0.0403	0.0278	0.0202
0.50	—	6.569	2.468	1.345	0.852	0.426	0.252	0.165	0.116	0.0855	0.0654	0.0415	0.0284	0.0205
0.00	—	7.806	3.039	1.594	0.973	0.462	0.266	0.171	0.119	0.0872	0.0664	0.0420	0.0286	0.0206
−0.50	—	6.566	2.466	1.343	0.851	0.425	0.252	0.165	0.116	0.0855	0.0654	0.0416	0.0285	0.0205
−1.00	—	1.590	1.136	0.803	0.584	0.340	0.217	0.149	0.108	0.0807	0.0625	0.0403	0.0278	0.0202
−1.50	0.547	0.498	0.489	0.428	0.360	0.249	0.176	0.128	0.0958	0.0738	0.0582	0.0384	0.0269	0.0196
−2.00	0.273	0.251	0.256	0.247	0.226	0.178	0.137	0.106	0.0828	0.0657	0.0530	0.0360	0.0256	0.0189
−2.50	0.166	0.154	0.155	0.156	0.149	0.129	0.106	0.0863	0.0702	0.0575	0.0475	0.0333	0.0241	0.0181
−3.00	0.112	0.106	0.104	0.106	0.104	0.0949	0.0824	0.0701	0.0591	0.0497	0.0420	0.030393	0.0226	0.0172
−3.50	0.0802	0.0767	0.0745	0.0759	0.0760	0.0719	0.0648	0.0571	0.0495	0.0428	0.0369	0.027559	0.0209	0.0162
−4.00	0.0604	0.0582	0.0561	0.0570	0.0575	0.0557	0.0517	0.0468	0.0416	0.0367	0.0322	0.024838	0.0193	0.0151
−5.00	0.0376	0.0366	0.0352	0.0353	0.0358	0.0357	0.0344	0.0323	0.0298	0.0271	0.0246	0.019982	0.0161	0.0131
−6.00	0.0255	0.0250	0.0242	0.0239	0.0242	0.0244	0.0240	0.0231	0.0218	0.0204	0.0189	0.016003	0.0134	0.0111
−7.00	0.0183	0.0180	0.0175	0.0172	0.0173	0.0175	0.0174	0.0170	0.0164	0.0156	0.0147	0.012847	0.0111	0.0094

To obtain cGy/mgRaEq-h, multiply table entries by 7.227.

$$\%\sigma_{\mathrm{RMS}}(\mu_1,\mu_2) = \sqrt{\sum_{i=1}^{N}\left(\frac{[\dot{D}_{\mathrm{wat},i}(r,\theta;\mu_1,\mu_2)/S_K]_{\mathrm{sievt}}}{[\dot{D}_{\mathrm{wat},i}(r,\theta)/S_K]_{\mathrm{MCPT}}} - 1\right)^2 \Big/ N}$$

$$(\hat{\mu}_1,\hat{\mu}_2) = \arg\min_{\mu_1,\mu_2}\{\%\sigma_{\mathrm{RMS}}(\mu_1,\mu_2)\} \qquad (2)$$

where N (= 317) denotes the number of data points in the Monte Carlo dose-rate distribution grid. This optimization procedure was performed with the 3M 6500 and CDCS.J (1982 design) sources.

The accuracy of several commonly used geometric approximations to the full 3D source structure for implementing the Sievert integral model was evaluated. These models included:

(a) Simulation of the 3D source geometry illustrated in Figs. 1 and 2.
(b) Right cylindrical core approximation: replacing the spherical glass bead array of the 1992 CDCS.J source by a right circular cylinder of ceramic preserving the active length, radius, and total mass of core material.
(c) Ceramic line-source approximation: replacing the finite radius core with a 0.02-mm-diameter cylindrical ceramic-filled cavity, reducing the stainless steel capsule radius to its radial thickness plus 0.01 mm and maintaining its symmetric or asymmetric positioning between the mechanical tip and end of the source.
(d) Steel line-source approximation: option (c) except that the needle-shaped active core cavity is assumed to consist of steel rather than ceramic.

Models (c) and (d) differ only along the longitudinal axis. Assuming that $\mu_2 \gg \mu_1$, model (c) predicts $\dot{D}(0, y) \propto (y^2 - L^2/4)^{-1} \cdot e^{-\mu_2 \cdot (P-L)/2}$ where P is the physical capsule length and L is the active length. In model (d) photons are attenuated along both the active length and capsule ends, resulting in a much larger filtration correction: $\dot{D}(0, y) \propto \int_{-L/2}^{L/2} (y - l)^{-2} \cdot e^{-\mu_2(0.5L-l)} \cdot dl$.

Models (c) and (d) describe commercial implementations of the 1D pathlength algorithm that ignore the lower-density core, approximate the radioactivity distribution by a line source, and model only the cylindrical capsule. Each of the models (a)–(d) was evaluated against MCPT calculations (based on full 3D geometry) for the 3M source, the 1982 CDCS.J source, and the 1992 CDCS.J source (measured dimensions) using linear energy absorption coefficients and best-fit values to evaluate the (μ_1,μ_2).

RESULTS

Dose rate per unit air kerma strength, as calculated by Monte Carlo simulation, is presented as a function of distances away (perpendicular distance from symmetry axis) and along (distance from source core center parallel to symmetry axis) in Tables 4–7 for the 1982-type Amersham CDCS.J source, the 1992 type CDCS.J source assuming the vendor's specifications, the 1992 CDCS.J source assuming

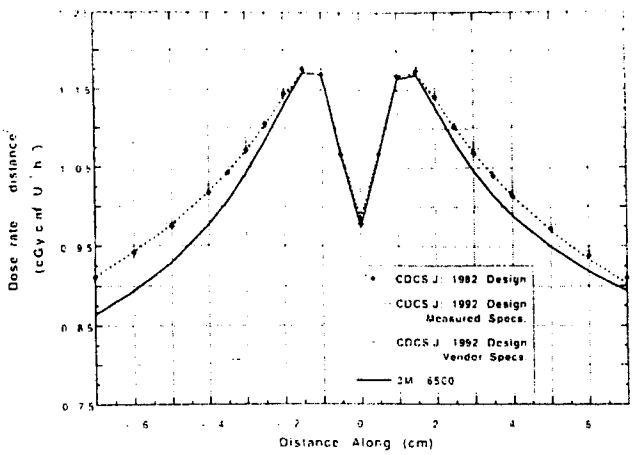

(a)

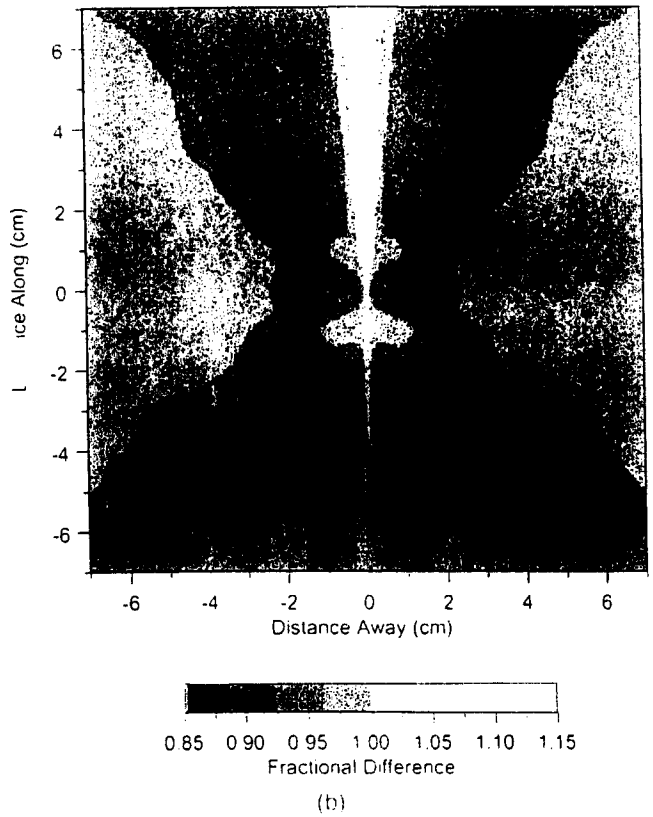

(b)

Fig. 4. (a) Dose-rate profiles for the 3M 6500 source, 1982 CDCS.J source, and 1992 CDCS.J source (vendor and measured geometry) derived from MCPT simulations. The product of dose rate and square of the distance is plotted along a line parallel to the source axis at 1 cm from the source center. The dose peaks centered at ±1.5 cm are artifacts of this effort to suppress inverse-square law. (b) 2D plot of the ratio of the 3M dose rate distribution to that of the 1992 design CDCS.J source, assuming measured geometrical specifications (Fig. 1c), as a function of location with respect to active source center. Both dose distributions were calculated by Monte Carlo simulation.

the average measured geometry, and the 3M model 6500 source. The RMS deviation of the 1982 CDCS.J dose distribution from that of the 1992 (measured geometry) design is 1.2% (range: −3.2% to +7.6%). Errors in excess of ±3% occur on or very near the longitudinal axis. Transverse-axis errors are limited to 1% at distances beyond 1 cm. The RMS deviation of the 1992 CDCS.J distribution (measured geometry) from that derived from the vendor's specifications is 1.2% (range: −2.5% to +6.2%). The 3M dose distribution differs from that of the CDCS.J tube (1992 design, measured geometry) by −5.9% to +14.4% (RMS mean: 2.6%) with the largest errors appearing near its longitudinal axis at the end opposite the eyelet (Fig. 4b). Figure 4a confirms that the three CDCS.J source types give rise to nearly identical dose-rate distributions at 1 cm distance, but differ significantly from that of the 3M 6500 source.

The origin of Tables 4–7 (away = 0 and along = 0) is located at the active source center, not at the center of the steel capsule. The negative "distance along" axis always points toward the eyelet end of the source. The table entries have units of cGy/h per unit $\mu Gy \cdot m^2 \cdot h^{-1}$ of air-kerma strength. To obtain dose rate per equivalent mass of radium (0.5 mm Pt), in units of cGy/mgRaEq-h, the table entries should be multiplied by the following factor:

$$[S_K/\text{mgRaEq}] = (\Gamma\delta)_{Ra}(0.5\text{ mm Pt}) \cdot (W/e) \quad (3)$$

$$= 8.25\ \frac{R \cdot cm^2}{mg-h} \cdot 0.876\ cGy/R$$

$$= 7.227\ \frac{\mu Gy \cdot m^2 \cdot h^{-1}}{mgRaEq}$$

Had the origin been placed at the physical source center, the dosimetric differences between sources with symmetrical and asymmetrically distributed radionuclides would have been substantially increased. For the 3M source, dose rates at polar angles of 0° and 180° would have differed by 23% had the origin been centered in the physical source (8).

Evaluation of the function $\%\sigma_{RMS}(\mu_1, \mu_2)$ shows that it is minimized at approximately the same location, $(\hat{\mu}_1, \hat{\mu}_2)$ in the 2D filtration coefficient parameter space for both the 1982 CDCS.J and 3M 6500 source designs. The optimal choice of steel filtration coefficient, $\hat{\mu}_2 = 0.0365\ mm^{-1}$, is significantly larger than the linear energy absorption coefficient for 662 keV photons ($0.0226\ mm^{-1}$). Use of the "best-fit" filtration coefficients averaged over the two source designs reduces the RMS mean errors to 0.7% and 0.8% for the 3M and 1982 Amersham source designs, respectively, with maximum errors ranging from −1.8% to +4.1%.

Filtration coefficients for implementing the 1D path-length model are listed in Table 3. The maximum and RMS average discrepancies between various implementations of this model and the more exact Monte Carlo calculations are listed in Table 8. For the 3M source and the 1982 CDCS.J source designs, approximating the filtration coefficients by linear energy absorption coefficients results in RMS average errors of 2.8% and 2.4%, respectively, with a maximum error of 7.6%. If the best fit filtration coefficients derived from fitting the 1D pathlength model to Monte Carlo sim-

Table 8. Accuracy of 1D pathlength model relative to Monte Carlo simulation

1D pathlength model type	Monte Carlo dose-rate distribution					
	CDCS.J 1982 source (Fig. 1a)		CDCS.J 1992 source (Fig. 1c)		3M 6500 source (Fig. 2)	
	% RMS Error	% Error Range	% RMS Error	% Error Range	% RMS Error	% Error Range
Average best fit (μ_1,μ_2) 3D geometry	0.8%	−0.95% to + 4.1%	0.7%	−1.7% to 4.2%	0.7%	−1.8% to +3.6%
Average best fit (μ_1,μ_2) bead array approximated by cylindrical core	—	—	0.9%	−1.4% to 4.0%	—	—
Average best fit (μ_1,μ_2) Ceramic line-source approximation	2.6%	−15.9% to 4.7%	2.7%	−16.0% to +5.2%	3.2%	−14.4% to 3.7%
Average best fit (μ_1,μ_2) Steel line-source	4.7%	−17.6% to +4.6%	4.4%	−16.7% to +5.0%	4.9%	−16.4% to +3.7%
$(\mu_1,\mu_2) = (\mu_{en,1}, \mu_{en,2})$ 3D geometry	2.5%	−1.4% to +6.0%	2.8%	−0.3% to +8.1%	2.8%	−1.2% to 7.6%
$(\mu_1,\mu_2) = (\mu_{en,1}, \mu_{en,2})$ Ceramic line-source approximation	2.8%	−5.5% to +8.1%	3.0%	−5.4% to 10.1%	2.7%	−5.2% to 9.2%
$(\mu_1,\mu_2) = (\mu_{en,1}, \mu_{en,1})$ Steel line-source approximation	3.0%	−6.9% to 8.0%	2.8%	−5.9% to +9.9%	3.0%	−7.2% to +9.2%

ulations for cylindrical core sources are applied to the measured CDCS.J 1992 geometry (including explicit modeling of the discrete glass spheres), a high level of accuracy (0.7% RMS error) is maintained.

Figure 5 illustrates the accuracy achieved by several 1D pathlength algorithm implementations, relative to MCPT simulation, as a function of position relative to the glass bead array center of the CDCS.J source. Assuming full 3D geometry, dose overestimates of 4–8% occur within a 30° cone centered about the longitudinal source axis when linear energy absorption coefficients are used to model filtration effects (Fig. 5a) whereas virtually no errors beyond ±3% occur when the best-fit filtration coefficients are used (Fig. 5b). When linear energy absorption coefficients are used in conjunction with the ceramic line-source model, the 4–8% overestimate cone widens to 40° and contains focal regions of −5% dose underestimate (Fig. 5c). Applying the best-fit filtration coefficients to the line-source model (Fig. 5d) results in a narrow 5–10% dose-underestimation cone. Even though the "best-fit line-source" model produces equivalent RMS deviations and larger maximum errors (Table 8) compared to the linear energy absorption coefficient approximation, the underdose cone is limited to about 12°. Figure 6 compares dose rates calculated by Monte Carlo simulation and several pathlength model implementations for the 3M model 6500 source. In the case of the ceramic line-source approximation, the best-fit filtration coefficients result in excellent agreement with Monte Carlo simulation in the 10°–170° polar angle range although errors close to the longitudinal axis are larger than when linear energy absorption coefficients are used.

Table 8 summarizes the Sievert integral accuracy results. Best-fit filtration coefficients in conjunction with an accurate 3D geometric model yield RMS errors of 0.7–0.8% for all source types while use of μ_{en} to model filtration results in errors 2.5–2.8%. Approximating the linear bead array of the 1992 CDCS.J by a uniform cylinder source does not affect 1D pathlength calculational accuracy. The ceramic line source models have the similar RMS errors (2.6–3.0%) for either choice of filtration coefficient, although the more detailed error maps (Figs. 5 and 6) suggest that best-fit filtration coefficients produce the best overall result. Replacing the ceramic line with a solid "steel" line does not influence model accuracy when μ_{en} filtration coefficients are used, but increases the RMS error to about 5% when best-fit values are used. The choice of steel or ceramic only influences doses on the longitudinal axes of the sources.

DISCUSSION

This paper presents the first detailed dose-rate distribution for the Amersham 1982 and 1992 versions of the CDCS.J intracavitary ^{137}Cs source. The latter is currently the only commercially available source for manually afterloaded intracavitary implants. In addition, updated dose-rate tables for the 3M model 6500/CDCK source have been provided. In contrast to previously published tables (6–8) derived from 1D path-

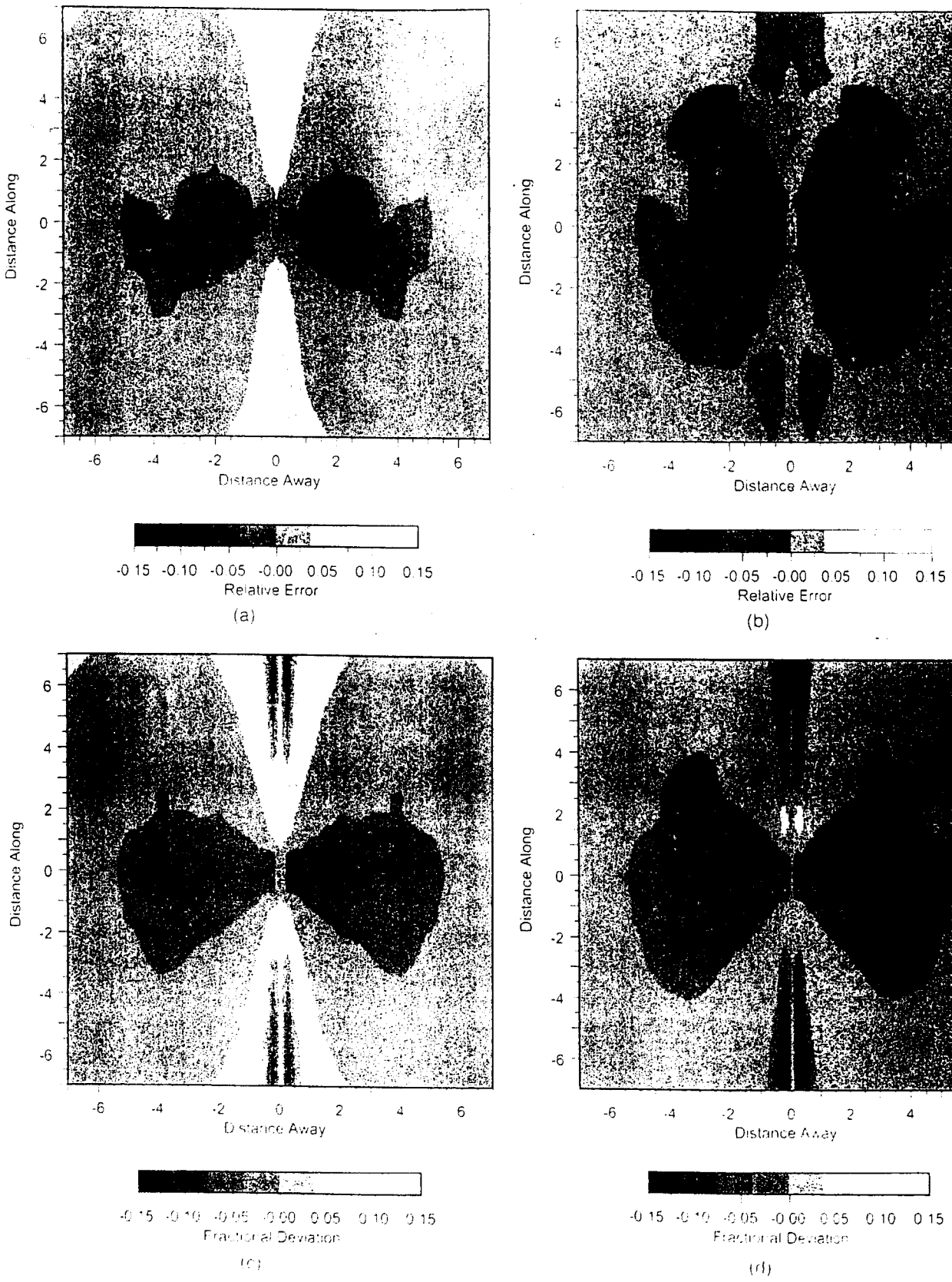

Fig. 5. Spatial distribution of fractional deviations of the 1D pathlength model calculations from Monte Carlo dose rate calculations for the Vari-Source CDCS I source (1992 version, measured geometry). (a) 1D geometry approximating filtration coefficients by [illegible] 1D geometry approximating filtration coefficients by [illegible] Ceramic line source model applied [illegible] attenuation coefficients by μ_{eff}. (d) Ceramic line source model applied [illegible] filtration coefficients [illegible].

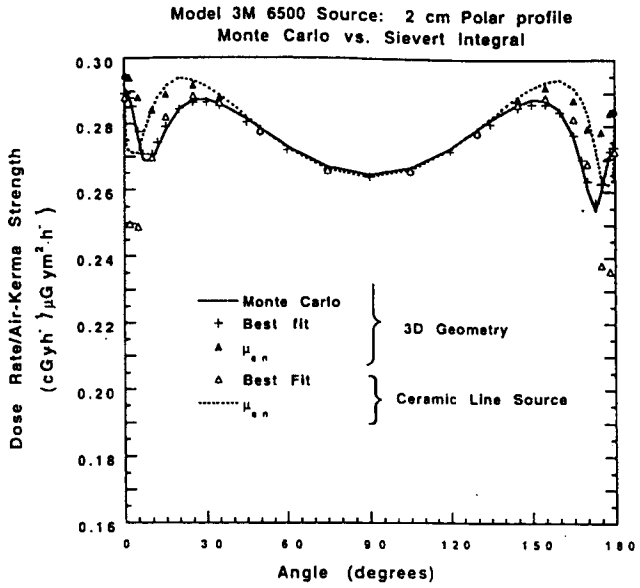

Fig. 6. Dose-rate as a function of polar angle at a fixed 2-cm distance from the active core center of a 3M Model 6500 source. Data derived from MCPT simulation as well as several implementations of the 1D pathlength model are shown.

length calculations, our tables are derived directly from a more fundamental experimentally validated Monte Carlo photon-transport code. The model CDCS.J dose distribution based upon radiographically measured average geometric dimensions was found to be in close agreement with the dose distribution based upon the vendor's geometric specifications. However, our measurements demonstrate that the internal dimensions of individual sources deviate from vendor specifications by as much as 1.8 mm. Of most dosimetric concern are unexpected deviations of the active core from its expected location in the source capsule. These findings underscore the importance of subjecting each new batch of intracavitary sources to rigorous radiographic examination before placing them in clinical service (2).

Tables 4 and 6 show that the maximum influence asymmetric positioning of the active source cavity in between the ends of the source capsule (1.6 mm and 1.0 mm for the 3M and Amersham sources, respectively) does not exceed 6% in contrast to Waggener (8) and Sharma (28) who found that the asymmetric 3M source design gave rise to dosimetric asymmetries in excess of 20%. These authors used a coordinate system centered on the source capsule (implying that the active source cavity is not centered on the origin) in contrast to our tables which assume that "distance along" is specified relative to the active source center. Readers should bear this convention in mind when applying our tables to practical problems.

The accuracy of several implementations of the 1D pathlength model (Sievert integral) has been assessed, assuming that Monte Carlo simulation accurately represents the true dose distribution around the source. The average accuracy of this simple algorithm is better than 1% if the filtration coefficients for the ceramic active core and steel encapsulation (μ_1 and μ_2) are treated as geometry-independent parameters of best fit. For both the 3M and Amersham sources, taking $\mu_2 = 0.036$ mm^{-1} (stainless steel) and $(\mu_1/\rho) = 0.0295$ cm^2/g (ceramic or glass), yields maximum and RMS average dose calculation errors of 4% and 0.8% over the 0.25 cm to 7 cm distance range. These findings are similar to those of Diffey (10) who found that $\mu_2 = 0.034$ mm^{-1} maximized the agreement between measured and calculated dose-rates for a CDC K-type source. Williamson (4) found that $\mu_2 = 0.039$ mm^{-1} maximized agreement between Monte Carlo and 1D pathlength calculations at a single fixed distance of 2 cm for a steel-clad cesium tube containing ^{137}Cs in ceramic pellets. Approximating the filtration coefficients by linear energy absorption coefficients (μ_{en}) resulted in RMS average errors of about 3% and maximum errors of 8%. For optimal accuracy near steel-clad, low-density core ^{137}Cs sources, the "best-fit" filtration coefficients should be used in conjunction with a three-dimensional geometric model. If the treatment planning system is limited to representing the source geometry by a line source embedded in a solid cylinder of steel, then mean accuracy will be limited to 3% regardless of whether linear energy absorption or the recommended "best-fit" filtration coefficients are used, although best-fit filtration coefficients accurately reproduce the Monte Carlo results over a larger range of solid angles. Even though all 1D pathlength algorithm variants perform accurately over the 30°–150° polar angle range, 8–15% dose calculation errors near the longitudinal source axis could be clinically significant for vaginal plaques or colpostats which align the source axes perpendicular to the coronal plane of the patient.

CONCLUSION

A Monte Carlo photon transport code has been used to calculate detailed dose-rate distributions in the form of a Cartesian lookup table for the two manual afterloading intracavitary ^{137}Cs tubes sources most widely used in the United States: the Amersham CDCS.J and the 3M model 6500/6D6C sources. The accuracy of the widely used 1D pathlength (Sievert integral) algorithm has been systematically assessed relative to Monte Carlo benchmark calculations. Its mean accuracy is better than 1% for a broad range of encapsulated ^{137}Cs sources containing low-density ceramic or glass matrix cores when optimal geometry-independent values of filtration coefficients for stainless steel and ceramic media are adopted.

REFERENCES

1. AAPM. Comprehensive QA for radiation oncology: Report of the American Association of Physicists in Medicine Radiation Therapy Committee Task Group 40. Med. Phys. 21:581–617; 1994.

2. Williamson, J. F. Practical quality assurance in low-dose rate brachytherapy. In: Starkshall, G.; Horton, J. L., eds. Proceedings of American College of Medical Physics–Sponsored Symposium on Quality Assurance in Radiotherapy Physics. Madison, WI: Medical Physics Publishing; 1991:139–182.
3. Young, M. E. J.; Batho, H. F. Dose tables for linear radium sources calculated by an electronic computer. Br. J. Radiol. 37:38; 1964.
4. Williamson, J. F. Monte Carlo and analytic calculation of absorbed dose near Cs-137 intracavitary sources. Int. J. Radiat. Oncol. Biol. Phys. 15:227–237; 1988.
5. Walz, R. N. A Study on the Use of Radium and Radium Substitutes in Brachytherapy. Natioanl Center for Radiological Health, Final Report, Contract PH 86-66-92, June, 1968, Washington, D.C.
6. Krishnaswamy, V. Dose distribution about ^{137}Cs sources in tissue. Radiol. 105:181–184; 1972.
7. Shalek, R. J.; Stovall, M. Dosimetry in implant therapy. In: Attix, F. H.; Tochlin, E., eds. Radiation Dosimetry, Vol. III. New York: Academic Press; 1969:776–798.
8. Waggener, R.; Lange, J.; Feldmeier, P.; Eagan, P.; Martin, S. Cs-137 dosimetry table for asymmetric source. Med. Phys. 16:305–308; 1989.
9. Metcalfe, P. E. Experimental verification of cesium brachytherapy line source emission using a semiconductor detector. Med. Phys. 15:702–706; 1988.
10. Diffey, B. L.; Klevenhagen, S. C. An experimental and calculated dose distribution in water around CDC K-type caesium-137 sources. Phys. Med. Biol. 20:446–454; 1975.
11. Williamson, J. F.; Meigooni, A. S. Quantitative dosimetry methods for brachytherapy. In: Williamson, J. F.; Thomadsen, B. T.; Nath, R., eds. Brachytherapy Physics. Madison, WI: Medical Physics Publishing; 1995:87–134.
Amersham International, plc. Caesium-137 and Radium-226 Sources for Brachytherapy. Buckinghamshire, England: The Radiochemical Centre/Amersham; 1972.
13. Amersham International, plc. Caesium-137 Stainless Steel Encapsulated Needle and Tube Sources for Interstitial and Intracavitary Brachytherapy. Buckinghamshire, England: Amersham International plc; 1982.
14. Ryan, J. (1964). Radioactive sources and method for making. Patent 3147225, United States Patent Office.
15. Kim, Y. S.; LaFave, J. W.; MacClean, L. D. The use of radiating microspheres in the treatment of experimental and human malignancy. Surgery 52:220–231; 1962.
16. Li, Z.; Williamson, J. F. Volume-based geometric modeling for radiation transport calculations. Med. Phys. 19:667–677; 1992.
17. Williamson, J. F. Monte Carlo evaluation of kerma at a point for photon transport problems. Med. Phys. 14:567–576; 1987.
18. Roussin, R. W.; Knight, J. R.; Hubbell, J. H.; Howerton, R. J. (1983) Description of the DCL-99/Hugo Package of Photon Interactions, Report ORNL/RSIC-46, Oak Ridge National Laboratory, Radiation Shielding Information Center, Oak Ridge, TN.
19. Hubbell, J. H. Photon mass attenuation and energy absorption coefficients from 1 keV to 20 MeV. Int. J. Appl. Radiat. Isot. 33:1269–1290; 1982.
20. NCRP. A Handbook of Radioactivity Measurements, NCRP Report No. 58. Bethesda, MD: National Council on Radiation Protection and Measurements; 1985.
21. Perera, H.; Williamson, J. F.; Li, Z.; Mishra, V.; Meigooni, A. S. Dosimetric characteristics, air-kerma strength calibration and verification of Monte Carlo simulation for a new ytterbium-169 brachytherapy source. Int. J. Radiat. Oncol. Biol. Phys. 28:953–971; 1994.
22. Williamson, J. F.; Perera, H.; Li, Z.; Lutz, W. R. Comparison of calculated and measured heterogeneity correction factors for I-125, Cs-137, and Ir-192 brachytherapy sources near localized heterogeneities. Med. Phys. 20:209–222; 1993.
23. Valicenti, R. K.; Kirov, A. S.; Meigooni, A. S.; Mishra, V.; Das, R. K.; Williamson, J. F. Experimental validation of Monte Carlo dose-calculations about a high-intensity Ir-192 source for pulsed dose-rate brachytherapy. Med. Phys. 22: 821–830; 1995.
24. Kirov, A. S.; Williamson, J. F.; Meigooni, A. S.; Zhu, Y. TLD, diode and Monte Carlo dosimetry of an Ir-192 source for high dose-rate brachytherapy. Phys. Med. Biol. 40:2015–2036; 1995.
25. Kirov, A. S.; Rogers, D. W. O.; Daskalov, G. M.; Williamson, J. F. Secondary electron transport in brachytherapy dosimetry: Evaluation of the dose-to-Kerma ratio for localized gamma sources (abstract). Med. Phys. 23:1065; 1996.
26. Williamson, J. F. The Sievert integral revisited: Evaluation and extension to ^{125}I, ^{169}Yb, and ^{192}Ir brachytherapy sources. Int. J. Radiat. Oncol. Biol. Phys. 36:1239–1250; 1996.
27. BIR/IPSM. (1993). Recommendations for Brachytherapy Dosimetry: Report of a Joint Working Party of the British Institute of Radiology and the Institute of Physical Sciences in Medicine. London: British Institute of Radiology.
28. Sharma, S. C.; Williamson, J. F.; Khan, F. M.; Jones, T. K. Dosimetric consequences of asymmetric positioning of active source in ^{137}Cs and ^{226}Ra intracavitary tubes. Int. J. Radiat. Oncol. Biol. Phys. 7:555–559; 1981.